Journal of The Electrochemical Society, **155** (11) B1194-B1201 (2008)
0013-4651/2008/155(11)/B1194/8/$23.00 © The Electrochemical Society

Investigation of Cathode Behavior of Model Thin-Film $SrTi_{1-x}Fe_xO_{3-\delta}$ ($x = 0.35$ and 0.5) Mixed Ionic-Electronic Conducting Electrodes

WooChul Jung[z] **and Harry L. Tuller***

Department of Materials Science and Engineering, Massachusetts Institute of Technology, Cambridge, Massachusetts 02139, USA

$SrTi_{1-x}Fe_xO_{3-\delta}$ (STF) model cathodes, with compositions $x = 0.35$ and 0.5, prepared as dense films with a well-defined area and thickness on top of a single-crystal yttria stabilized zirconia substrate by pulsed layer deposition at 700°C were investigated by electrochemical impedance spectroscopy as a function of electrode geometry, temperature, and oxygen partial pressure. The STF cathode was observed to exhibit typical mixed ionic-electronic behavior with the electrode reaction occurring over the full electrode surface area rather than being limited to the triple-phase boundary. The electrode impedance was observed to be independent of electrode thickness and inversely proportional to the square of the electrode diameter pointing to surface exchange limited kinetics. Furthermore, a $Ce_{0.9}Gd_{0.1}O_{2-\delta}$ interlayer was found to have no effect on the electrode impedance. Values for the surface exchange coefficient, k, were calculated and found to be comparable in magnitude to those exhibited by other popular mixed ionic-electronic conductors, such as $(La,Sr)(Co,Fe)O_3$, thereby, confirming the suitability of STF as a model-mixed conducting cathode material. The observed trends are discussed in relation to the known defect and transport properties of STF.
 [DOI: 10.1149/1.2976212]

Manuscript submitted June 20, 2008; revised manuscript received July 30, 2008. Published September 24, 2008.

Growing concerns have been recently generated regarding the ready availability of hydrocarbon fuels and the environmental impact associated with their combustion for power generation and vehicular applications. Fuel cells, offering higher fuel efficiencies and reduced emissions, have therefore been receiving increased attention. Among the various types of fuel cells, the solid oxide fuel cell (SOFC) is particularly attractive given its fuel flexibility (hydrocarbons, hydrogen, or even CO) and high conversion efficiencies enabled by its relatively high operating temperature (800–1000°C).[1] A key factor hindering SOFC development, however, is the inadequate degree of understanding regarding the kinetics controlling the cathode processes and the resultant inability to further reduce cathode polarization loss. This is particularly true when it comes to microfabricated SOFC and other SOFCs designed to operate at reduced temperatures (<600°C), wherein the cathode polarization loss often becomes the greatest obstacle toward achieving adequate electrochemical performance.[2]

Although there have been numerous research efforts directed toward understanding the electrode reaction mechanisms, they remain unsatisfactory and their conclusions controversial.[3-6] This may follow from the fact that the large majority of SOFC-related cathode studies have been complicated by the use of complex electrode morphologies.[3,7-10] In addition, the commonly used cathode materials, such as $(La,Sr)CoO_3$ (LSC) and $(La,Sr)(Co,Fe)O_3$ (LSCF), while they exhibit high levels of mixed ionic and electronic conductivities (MIEC), key parameters remain difficult to control (e.g., electronic and ionic conductivities and transference numbers, morphology, and chemical stability).[11-14] In this study, a perovskite materials system is selected for study, offering the ability to systematically control both the levels of ionic and electronic conductivity as well as the band structure. This, in combination with considerably simplified electrode geometry, is demonstrated to provide improved insight into the SOFC cathode processes.

Geometrically simple and reproducible dense, thin-film model electrode structures, fabricated by vacuum-based physical vapor deposition (PVD) methods, were recently reported by several researchers.[15-18] In this manner, both triple-phase boundary (TPB) length (TPBL) and area could be well defined, thereby allowing for a quantitative analysis of the electrochemical properties by normalization of the experimental data with respect to geometry, such as TPBL, surface area, film thickness, and surface roughness. Furthermore, films grown by PVD allow for the control of the electrode microstructure more precisely. Features such as crystal orientation, grain size and shape, and compositional variations, can be varied by control of deposition conditions (i.e., deposition temperature, pressure, power, gas composition, substrate composition, etc.).

The $SrTi_{1-x}Fe_xO_{3-\delta}$ (STF) system was chosen as a model cathode material in this study. STF forms a continuous solid solution over the entire composition range $0 < x < 1$ between the end members strontium titanate ($SrTiO_3$) and strontium ferrite ($SrFeO_3$).[19] Whereas strontium titanate is a wide-bandgap semiconductor ($E_g^o = 3.2$ eV at $T = 0$ K) with rather low conductivity levels in the undoped state,[20] systematic substitution of Fe for Ti, results in a systematic decrease in bandgap and an increase in electron, hole, and oxygen vacancy density, providing, in turn, mixed conductivity with high levels of electronic and ionic conductivities.[21] Both end members have been studied for some time,[20,22] and the STF system has received recent attention given its suitability as a lean burn engine exhaust sensor[23] and hydrocarbon sensor.[24] This has led to a detailed examination of its defect and transport properties.[21]

From the perspective of this study, the most important advantages of STF as a model cathode material is the ability to control both the magnitude and ratios of electronic and ionic conductivity and its stability over a wide range of pO_2 and temperature. In contrast to the typical MIEC cathode, such as $(La,Sr)CoO_3$ and $(La,Sr)(Co,Fe)O_3$, it is possible to vary both the ionic and electronic conductivity in STF by nearly five orders of magnitude (as shown in Fig. 1) by change of the Fe fraction. This offers the opportunity to control and ultimately develop a deeper understanding of the role that these key material parameters play in influencing cathode behavior.

In this initial study of STF as a SOFC cathode, electrochemical impedance spectroscopy (EIS) is employed to assess where the critical active sites reside. Specifically, the question of whether the rate limiting steps are limited to the TPB, or over the whole electrode surface area, is considered. Furthermore, if the reactions are indeed spread across the electrode area, as might be expected for a MIEC material, are they governed by surface exchange, mass transfer through the electrode, or interfacial transfer between the STF electrode and the yttria-doped zirconia (YSZ) electrolyte? Here, advantage is taken of variations in film thickness and the introduction of intervening layers between electrolyte and electrode to assist in confirming a surface exchange limiting process. This provides the opportunity to calculate the oxygen surface exchange coefficient k, and compare it to values reported for popular MIEC cathode materials. The temperature and pO_2 dependence of the impedance results are

* Electrochemical Society Active Member.
[z] E-mail: wcjung@mit.edu

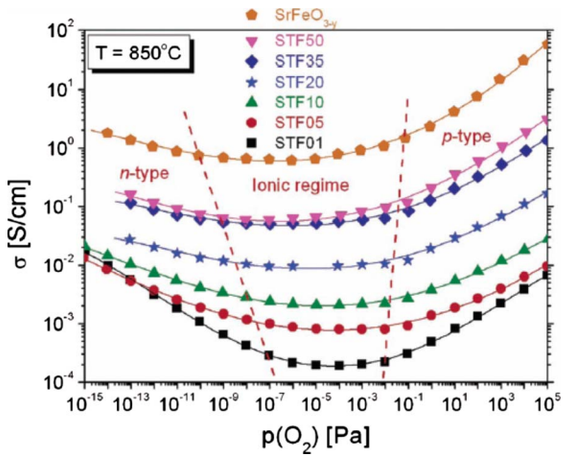

Figure 1. (Color online) Electrical conductivity (σ) isotherms, at T = 850°C, as a function of oxygen partial pressure (pO_2) for different bulk ceramic STF compositions with Fe concentration between 1 mol % (STF01) and 50 mol % (STF50), as well as $SrFeO_{3-y}$. (Reprinted with permission from Ref. 21. Copyright 2006 American Chemical Society.)

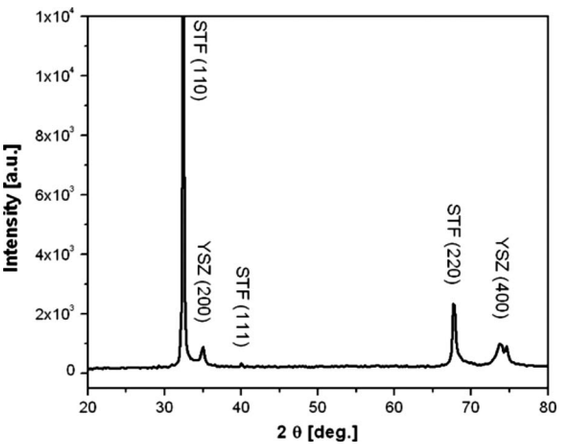

Figure 3. X-ray diffraction pattern of a 320 nm thick $SrTi_{0.5}Fe_{0.5}O_{3-\delta}$ film deposited on a YSZ single crystal with (100) orientation by PLD. The pattern indicates preferred (110) orientation with a small amount of (111) reflection.

analyzed, and the chemical capacitance of the STF electrode is discussed in terms of the appropriate thermodynamic data. Lastly, the possible roles played by the electronic and ionic conductivities in influencing cathode behavior are briefly discussed.

Experimental

STF thin films were prepared by means of pulsed-laser deposition (PLD) from oxide targets of the respective materials and deposited onto (100)-oriented single-crystal YSZ substrates (10 × 10 × 0.5 and 15 × 15 × 0.5 mm^3, MTI Corporation, Richmond, CA) as shown in Fig. 2. The oxide targets with 1 in. diameter were prepared by the conventional mixed-oxide technique, starting from iron (III) oxide (Alfa Aesar, 99.945%), strontium carbonate (Alfa Aesar, 99.99%), and titanium (IV) oxide (Alfa Aesar, 99.9%) powders. The powders were mixed to obtain the desired Fe/Ti ratios, ballmilled for 10 h, and subsequently calcined in air at 1250°C for 5 h. The targets were prepared by uniaxial pressing at 23 MPa followed by cold isostatic pressing at 275 MPa. The compacts were sintered at 1425°C for 5 h. The PLD system was operated with a KrF excimer laser, emitting at 248 nm (Coherent COMPex Pro 205), at energy of 500 mJ/pulse and with a repetition rate 15 Hz. The substrates were heated to 700°C during deposition, while the oxygen pressure was maintained at 5 mTorr after pumping the background pressure down to less than 3 × 10^{-6} Torr. Following deposition and prior to cooling, the oxygen pressure in the chamber was increased to approximately 6–7 Torr to facilitate more complete oxidation of the films. In some cases, a~50 nm thick interlayer of $Ce_{0.9}Gd_{0.1}O_{2-\delta}$ (CGO) was deposited between the YSZ electrolyte and the STF electrode, by reactive radio-frequency (rf) sputtering from an oxide target (deposition temperature, 300°C; oxygen pressure, 0.6 mTorr; rf power, 45 W).

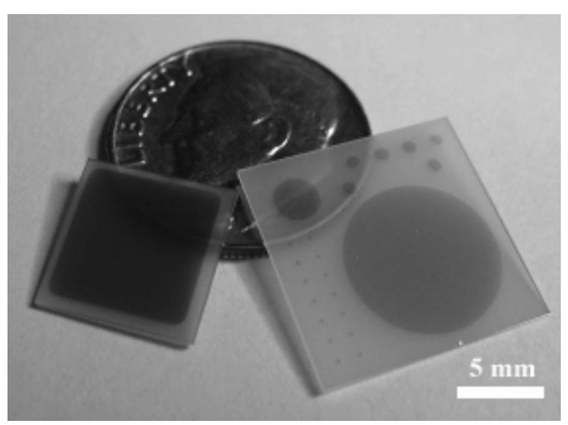

Figure 2. Photograph of STF thin films deposited by PLD. One square (9 × 9 mm) and four circular electrodes (1–10 mm diam) can be seen on top of a single-crystal YSZ substrate.

The resulting polycrystalline films exhibited the perovskite structure with highly (110)-orientated texture as confirmed by X-ray diffraction (Rigaku RU300); see Fig. 3. Grain sizes of between 100 and 200 nm and surface roughness of ~2 nm were measured by atomic force microscopy (Digital Instruments Nanoscope IIIa) while film thicknesses ranging between 70 and 440 nm were determined by surface profilometry (Tencor P-10).

Two different sample geometries were prepared for EIS measurements: a symmetrical structure with identically sized (9 × 9 mm) STF electrodes on both sides of the YSZ electrolyte, and an asymmetrical structure (1–10 mm diam STF electrode) in which a large porous Ag counter electrode (SPI Silver Paste Plus, SPI Supplies, Chester, PA, USA) was applied to one side of the YSZ electrolyte as shown in Fig. 4. In both cases, Au mesh and Au paste were placed on the top of the STF electrode surface serving as a current collector. Both a custom-designed enclosed probe station, manufactured by McAllister Technical Services (Coeur d'Alene, ID, USA) and a tube furnace were used for the EIS measurements at temperatures between 570 and 650°C and oxygen partial pressures between 2 × 10^{-5} and 1 atm. The pO_2's were controlled by preparing N_2 and O_2 gas mixtures with the aid of mass flow controllers and monitored by an in situ YSZ sensor. EIS measurements, covering the frequency range from 7 to 1 MHz with an amplitude of 20 mV were performed with Solarton 1260 or 1250 impedance analyzers operated in combination with a Solartron 1286 potentiostat.

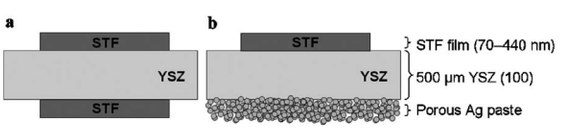

Figure 4. Schematic illustrations of the two different sample geometries: (a) a symmetrical structure with identically sized STF electrodes (9 × 9 mm) on both sides of the YSZ electrolyte, and (b) an asymmetrical structure (1–10 mm diam STF electrode) in which a large porous Ag counter electrode was applied to one side of the YSZ electrolyte.

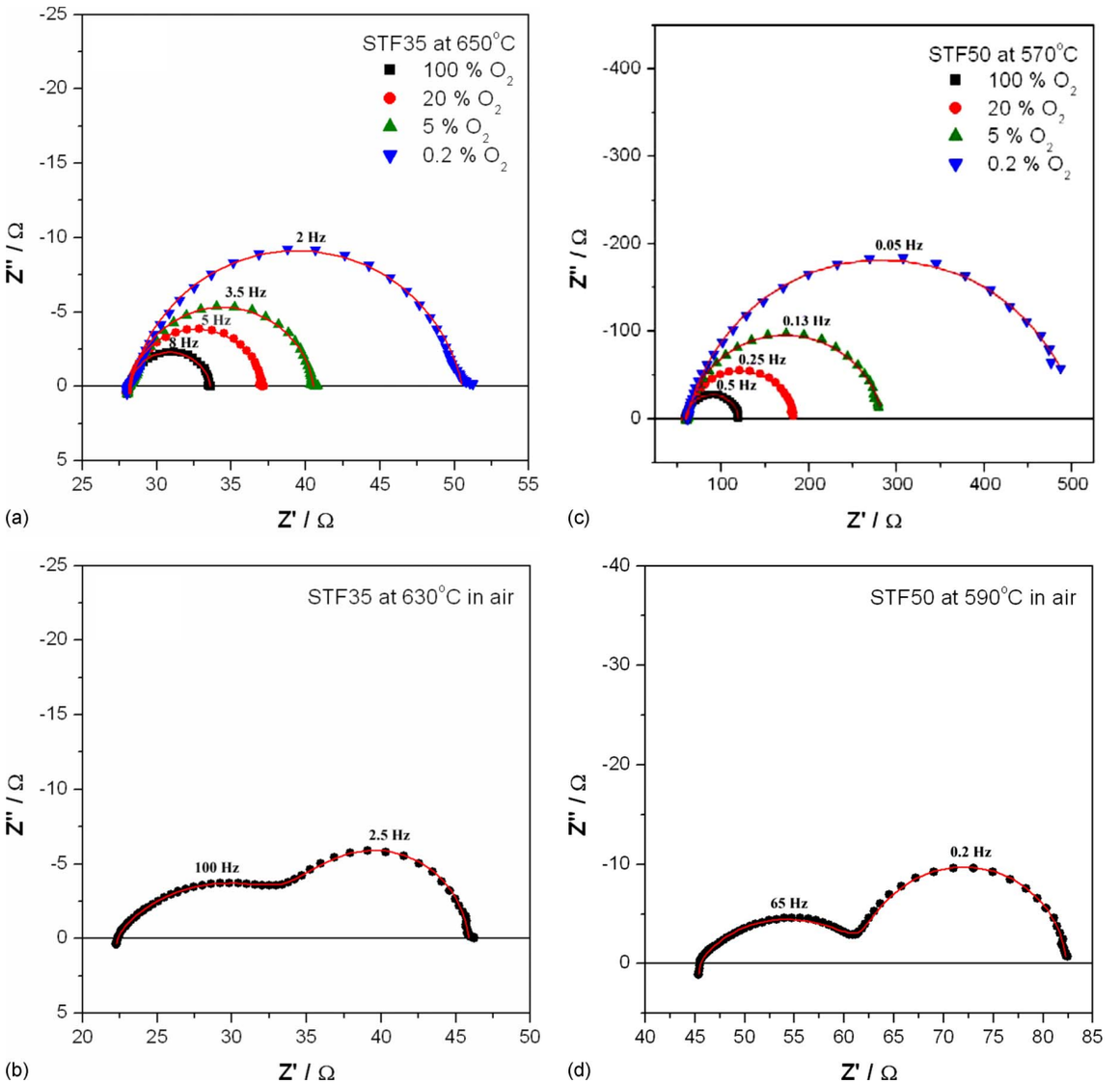

Figure 5. (Color online) Typical impedance spectroscopy plots of (a) a symmetric cell of STF35 at $T = 650°C$, (b) an asymmetric cell of STF35 at $T = 630°C$, (c) a symmetric cell of STF50 at $T = 570°C$, and (d) an asymmetric cell of STF50 at $T = 590°C$. All of the impedance spectra were measured in air.

Results

Figure 5 shows typical impedance results obtained for both the symmetrical and asymmetrical structure in which the STF electrodes were of composition $x = 0.35$ or 0.5 designated as STF35 or STF50, respectively. The symmetrical structure exhibits an offset resistance (R_{off}) and a nearly ideal semicircle, while the asymmetrical structure with the porous Ag counter electrode shows an offset resistance and two adjacent semicircles, which are distinguished as a more highly distorted high-frequency and a nearly ideal low-frequency semicircle, respectively.

In Fig. 6, the offset resistance of the STF35 for the two types of cells is plotted as log R vs $1/T$ with the two sets of data characterized by activation energy (Ea) of 0.96 ± 0.02 and 0.94 ± 0.02 eV, respectively. In Fig. 7, the STF35 offset resistance for the two types of cells is plotted as log R_{off} vs log pO_2 and within experimental error; one finds that this resistance is independent of pO_2. The impedance spectra of the STF50 also shows a similar temperature and pO_2 dependence for the offset resistance. As discussed later, this contribution is attributed to the YSZ ohmic contribution.

Focusing next on the symmetrical cell, given the near-ideal semicircular shape of the spectra at reduced frequency in Fig. 4a, one can assign this response to that expected from a parallel resistor-capacitor (R-C) circuit. For this work, the capacitor is replaced by a more general constant phase element, for which the impedance is given by

$$Z = \frac{1}{Q(i\omega)^n} \quad [1]$$

Applying the expression for a true capacitance according to Ref. 25 one obtains

$$C = Q\omega_{max}^{n-1} = (R^{1-n}Q)^{1/n} \quad [2]$$

This corresponds to a C value of ~12 mF/cm^2 for a 160 nm STF50 at 650°C (a typical n value is between 0.92 and 0.99.) This exceptionally high capacitance can only be that associated with the STF electrode. The R and C values derived from this part of the impedance spectra are therefore designated as R_{STF} and C_{STF}. In the fol-

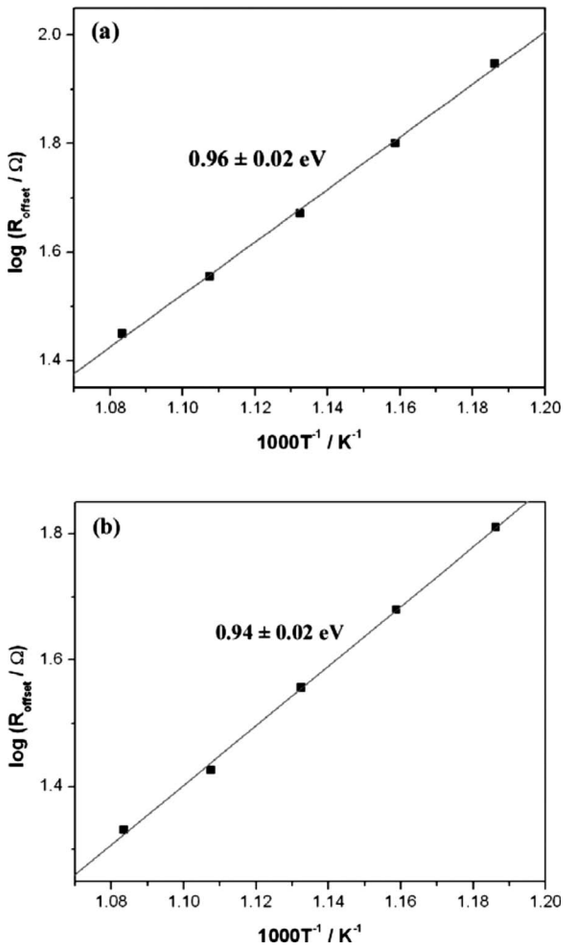

Figure 6. Temperature dependence (Arrhenius plots) of R_{off} for STF35, measured from (a) a symmetric cell and (b) an asymmetric cell in air.

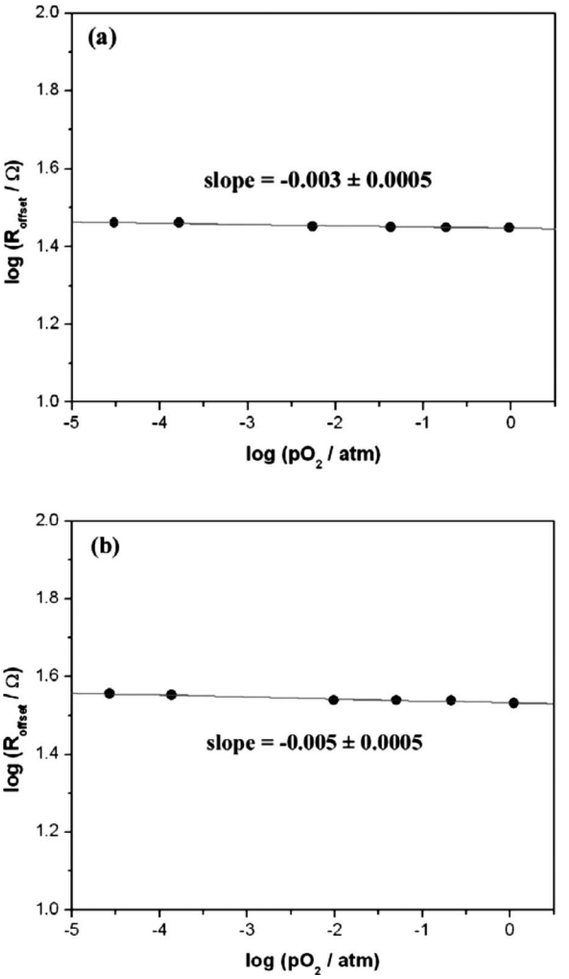

Figure 7. Oxygen partial pressure (pO_2) dependence of the R_{off} for STF35, measured from (a) a symmetric cell at 650°C and (b) an asymmetric cell at 610°C.

lowing, the geometrical, temperature, and pO_2 dependences of these parameters are examined.

Log R_{STF} and log C_{STF} for STF50 are plotted vs log electrode diameter in Fig. 8 and show a power law dependence of -2.27 ± 0.22 and 2.26 ± 0.21, respectively. In Fig. 9, log R_{STF} and log C_{STF} are plotted instead vs log electrode thickness. Here, the respective power laws were found to be -0.03 ± 0.09 and 0.98 ± 0.27, respectively. STF35 shows a similar geometrical dependence as STF50. The temperature dependence of R_{STF} for STF50 is examined at two different atmospheres in Fig. 10. The activation energies were found to be 1.82 ± 0.04 and 1.44 ± 0.08 eV at 0.2 and 10^{-4} atm, respectively. The pO_2 dependence of R_{STF} for STF35 and STF50 is plotted in Fig. 11 and show a decrease in R_{STF} with increasing pO_2 as commonly observed for perovskite-based cathodes. The pO_2 dependence, in turn, consistently increases with decreasing temperature for both STF35 and STF50 as shown in Table I.

Figure 12 compares the impedance of STF50 measured in air at 650°C for asymmetric cells with and without the CGO layer between the YSZ electrolyte and the STF electrode. The results, within experimental error, are identical suggesting that the interfacial CGO layer has little impact on electrode performance.

Discussion

Origins of impedance spectroscopy contributions.— In order to understand the origins of each contribution, it is helpful to examine the dependence of the impedance spectra on temperature and pO_2. Several features of the offset resistance are consistent with the source being the YSZ electrolyte single-crystal substrate. This includes the activation energy of R_{off} of ~0.95 eV and its pO_2 independence. Furthermore, the magnitude of conductivity (0.24×10^{-3} S/cm at 650°C), calculated based on the present cell electrode geometry, electrolyte thickness, and measured R_{off}, agree with the literature data for YSZ ionic conductivity (0.53×10^{-3} S/cm).[26] Lastly, R_{off} was found to be independent of cell structure (i.e., symmetric vs antisymmetric) and electrode composition STF35 vs STF50. One can thus confidently conclude that this impedance feature should be attributed to the YSZ electrolyte.

Given that the impedance spectra of the symmetric structure contains only a nearly ideal semicircle, this feature can be assigned to the STF electrodes, whereas for the asymmetric structures (which exhibit both a distorted and a nearly ideal semicircle), one can conclude that the more highly distorted high-frequency (HF) semicircle should be attributed to the Ag porous electrode while the nearly ideal low-frequency (LF) semicircle should be attributed to the STF electrode. For further confirmation, the activation energies of each semicircle in both structures were examined; both LF semicircles had the same Ea of 1.8–2.0 eV, while the HF one in the asymmetrical structure exhibited values of 1.1–1.2 eV. The area-specific resistance (ASR) of the LF semicircle from both structures was also compared, demonstrating they are the same within an error of ~13% for STF50 at 650°C. Therefore, one can confidently con-

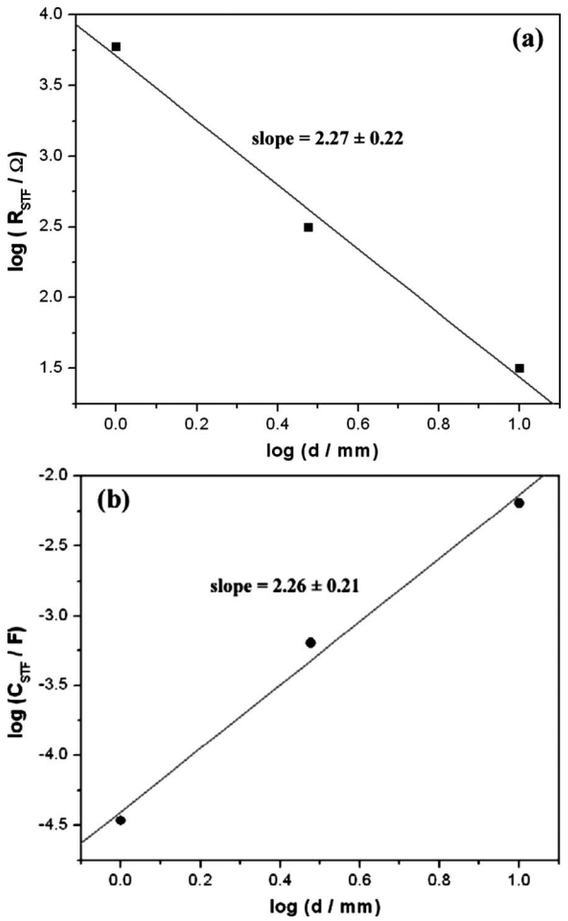

Figure 8. Double-logarithmic plots of the (a) R_{STF} and (b) C_{STF} of a STF50 electrode vs its diameter measured at 590°C in air using asymmetrical cells.

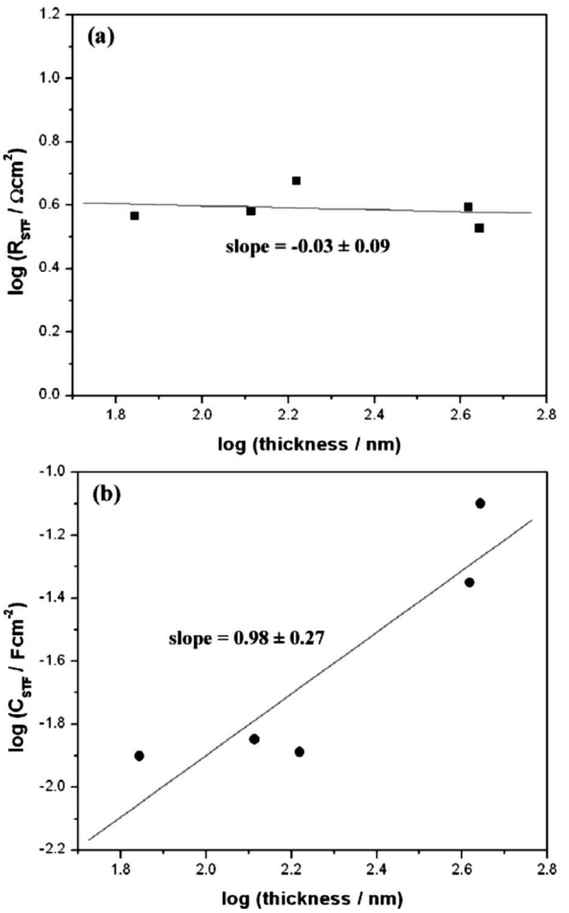

Figure 9. Double-logarithmic plots of the (a) R_{STF} and (b) C_{STF} of a STF50 electrode vs its thickness measured at 650°C in air.

clude that the highly distorted HF semicircle and the nearly ideal LF semicircle are attributed to the porous Ag counter electrode and the STF electrode, respectively.

Figure 12 shows no significant change in electrode impedance when a CGO layer was deposited between the YSZ electrolyte and the STF electrode. The purpose of the CGO layer is to modify the interfacial characteristics between a YSZ electrolyte and a STF electrode. If the corresponding interfacial impedance is significant, one can expect changes in the impedance spectra by the addition of a CGO interlayer. In this work, however, the impedance remains essentially the same, suggesting that the impedance of STF is not governed by the interfacial transfer. Utilization of the CGO interlayer for SOFC applications can be found in the literature, where it is reported that the CGO interlayer reduces the cathodic polarization loss[27] and that CGO is less reactive with perovskite oxides than YSZ preventing the formation of less conductive reaction products such as $La_2Zr_2O_7$.[28] In contrast to this work, interfacial impedances were observed in other studies of mixed conducting perovskite electrodes on YSZ.[15,18,29] The negligible interfacial impedance may result from the fact that the electrochemical cells in the present study have been maintained, at all times, at temperatures of <700°C, thereby resulting in negligible reaction products forming between the STF electrode and YSZ electrolyte or that STF is inherently more stable in contact with YSZ than other perovskite-based electrode materials (e.g., LSC). More systematic studies regarding the chemical compatibility of YSZ and STF thin films at reduced temperatures (<700°C) are planned for the future.

Active reaction sites.— In a mixed conducting electrode, oxygen reduction can take place either at the TPB between electrode, electrolyte, and gas phase or, for a dense electrode, at the surface of the electrode corresponding to the double-phase boundary between electrode and gas phase. The use of dense thin-film electrodes with simple geometry enables one to obtain a quantitative relationship between electrode impedance and geometry. In this study, a power-law dependence of ~ 2 (2.27 ± 0.22) obtained between electrode diameter (1–10 mm) and impedance (see Fig. 8) indicates that the measured values (R_{STF} and C_{STF}) are proportional to the electrode surface area, rather than to the TPBL for which one would expect instead of a power dependence of unity. One can thus conclude that the oxygen reduction reaction largely occurs over the electrode surface area of STF35 and STF50, rather than being limited to the TPB, as also reported for the thin-film LSC and LSCF MIEC electrodes.[18,29]

Surface exchange limited kinetics.— Three possible limiting processes can be related to the pathway passing through the electrode surface: (*i*) surface exchange at the electrode-gas interface, (*ii*) mass transport through the electrode, and (*iii*) interfacial transfer between the electrolyte and the electrode. If bulk mass transport is relevant, one would expect a significant deviation from the semicircular shape for the STF electrode impedance[30] and R_{STF} would be proportional to electrode thickness. However, the nearly ideal-shaped semicircle observed for the STF electrode in the complex impedance plane suggests that mass transfer is not the limiting process. This conclusion is further confirmed by the observed independence of R_{STF} on electrode thickness, as shown in Fig. 9. Further-

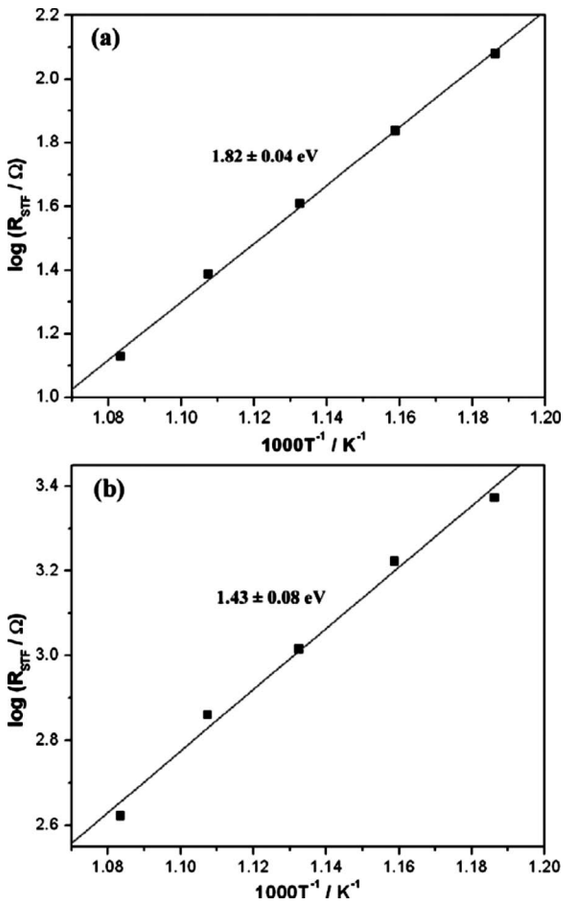

Figure 10. Temperature dependence (Arrhenius plots) of the R_{STF} of a STF50 electrode measured (a) in air and (b) in 100 ppm O_2.

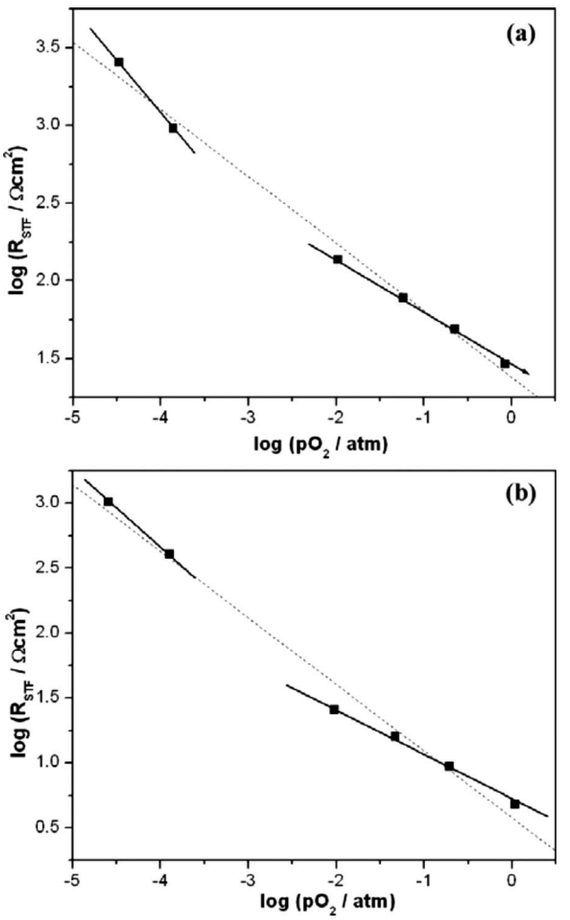

Figure 11. Double-logarithmic plots of the R_{STF} of a STF electrode vs pO_2: (a) a STF35 electrode measured at 570°C and (b) a STF50 electrode measured at 630°C.

more, as pointed out above, the electrode impedance was also found to be insensitive to the insertion of the CGO interlayer between the electrolyte and the STF electrode, as shown in Fig. 12. This supports the conclusion that the interfacial transfer between the STF electrode and YSZ electrolyte is not the rate-determining step. One can only conclude, therefore, that the limiting process in this study must be attributed to the surface oxygen exchange reaction occurring at the surface of the STF35 and STF50 electrodes.

In contrast to R_{STF}, C_{STF} shows a near linear (0.98 ± 0.27) dependence on STF electrode thickness; see Fig. 9. This suggests that the main capacitive feature of the STF impedance is proportional to electrode volume [proportional to both electrode diameter (Fig. 8) and thickness (Fig. 9)]. Furthermore, it is also independent of the CGO interlayer (Fig 12). This suggests that C_{STF} is a chemical capacitance, as discussed below.

Values for ASR and surface exchange coefficient.— Because the surface exchange reaction has been identified as being the limiting process, the corresponding kinetic parameter can now be extracted from the measured electrode resistance. According to a literature,[31] the surface oxygen exchange coefficient is inversely proportional to the resistance as

$$k^q = \frac{kT}{4e^2 R_S c_O} \quad [3]$$

where k is the Boltzmann constant, e is the electron charge, T is the temperature, R_s is the ASR, and c_O is the total concentration of lattice oxygen with the value 4.92×10^{22} cm^{-3} used in this calculation.[21]

Calculated k^q values, averaged from over six different STF50 samples and three different STF35 samples and extrapolated to 800°C, are shown in Table II. The calculated STF surface oxygen exchange coefficients are higher than those reported for the more typical MIEC cathodes, such as LSC and LSCF. This is perhaps surprising given that the electronic conductivity of the STF cathodes is nearly 200 times lower than those of LSC and LSCF at 800°C.

Further confirmation of surface exchange control can be obtained by examining the so-called characteristic thickness L_C, at which mass transport through the electrode thickness becomes dominant relative to the surface exchange reaction.[32] The characteristic thickness is defined as the ratio of the oxygen diffusion coefficient and the corresponding surface exchange coefficient, $L_C = D/k$. Values for the oxygen diffusion coefficient are derived from an analysis of

Table I. The pO_2 dependence of the electrode resistances for STF35 and STF50 at high oxygen partial pressure ($>10^{-3}$ atm) in the temperature range of 570–650°C.

Temp (°C)	STF50	STF35
650	−0.26 ± 0.03	−0.21 ± 0.03
630	−0.36 ± 0.01	−0.25 ± 0.03
610	−0.38 ± 0.04	−0.29 ± 0.01
590	−0.40 ± 0.01	−0.32 ± 0.01
570	−0.43 ± 0.02	−0.35 ± 0.01

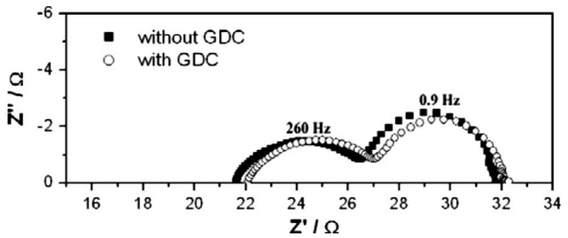

Figure 12. Comparison of two impedance spectra, one measured from asymmetric STF50 structures without a CGO interlayer (solid quadrangles) and with a CGO interlayer (open circles) at 650°C in air. The identical results, within experimental error, suggest that the interfacial CGO layer has little impact on the electrode performance.

electrical conductivity measurements performed on STF,[21] while the surface exchange coefficients are calculated from the EIS results in this work with the aid of Eq. 3. The characteristic thickness of STF35 and STF50 at 700°C (by extrapolation from 650°C) is roughly 200 and 250 μm, respectively, much thicker than the STF film thicknesses used in this work. Furthermore because L_C becomes thicker with decreasing temperature, given the larger activation energy of k than D, it is clear that the surface exchange reaction remains dominant in the temperature range of this work, 570–650°C.

The ASR obtained for dense thin films of the other MIEC electrodes by PLD are compared in Fig. 13 with the values obtained in this study for STF. This was done to insure that morphology differences between typical bulk MIEC electrodes and the dense thin film STF electrodes used in this study played no role in influencing performance. Again, the ASR values for STF are lower than those of LSC and LSCF pointing to the suitability of STF as a realistic model mixed conducting cathode material.

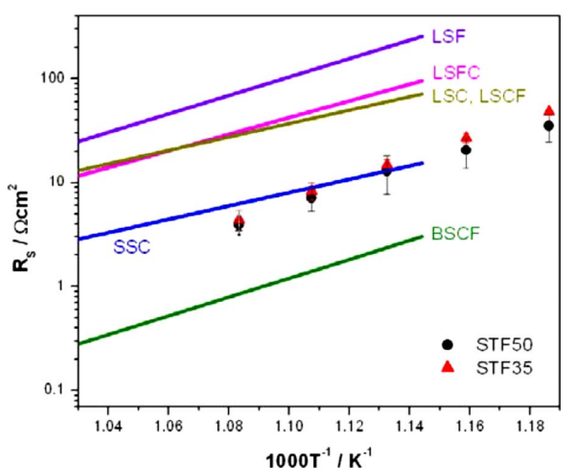

Figure 13. (Color online) Temperature dependence of ASR for STF35 (solid triangles), STF50 (solid circles), and other dense thin-film MIEC electrodes fabricated by PLD (straight lines). The data of other MIEC electrodes are obtained from the work of Baumann et al.[18]

Table III. Activation energies for STF35 and STF50 obtained from impedance measurements in the temperature range of 570–650°C at different oxygen partial pressures.

pO_2	Ea (eV) for STF35	Ea (eV) for STF50
Low ($<10^{-3}$ atm)	1.2–1.4	1.1–1.2
High ($>10^{-3}$ atm)	1.8–2.0	1.9–2.0

Generally speaking, it has been reported that both high σ_{el} and σ_{ion} guarantee fast surface exchange reactions,[5,33] although available kinetic and transport data remain limited and the relative roles of σ_{el} and σ_{ion} are not clearly explained. However, it is reasonable to conclude that σ_{el}, at least above a certain minimum value, does not play the limiting role in the surface exchange reactions of both STF and LSCF, according to the results in Table II.

Temperature and pO_2 dependence.— Figure 10 shows the temperature dependence of the STF electrode resistance. The activation energy is 2.00 ± 0.16 and 1.80 ± 0.14 eV for STF35 and STF50, respectively in air; see Table III. These are close to the values reported for $(Ba,Sr)(Co,Fe)O_3$ (BSCF) and $(La,Sr)FeO_3$ (LSF) (1.8 eV), but higher than that reported for LSC and LSCF (1.3–1.6 eV).[29] It should be noted that the activation energy has a pO_2 dependence; the activation energy of the STF impedance remains constant (1.8–2.0 eV) with changing pO_2 (0.01, 0.05, 0.2, and 1 atm), as long as the pO_2 remains $>10^{-3}$ atm. Below this pO_2, the activation energy drops to 1.2–1.4 eV (see Fig. 11). This suggests that there is a transition in the rate limiting process at around $pO_2 = 10^{-3}$ atm. More systematic studies will be required to clarify this effect further.

The pO_2 dependence of the electrode resistance is shown in Fig. 11 with the slope listed in Table I. The slope is close to one quarter with some variation at different temperatures and Fe concentrations, a value close to that reported (0.27—0.31) for lightly Fe-doped (0.13%) $SrTiO_3$.[34] Consistently, the pO_2 dependence increases with decreasing temperature for both STF35 and STF50. The reason for this trend is still unclear and under further investigation.

Chemical capacitance.— The capacitance is dependent on the electrode volume and its magnitude is extremely high (12 mF/cm^2 at 160 nm), which is consistent with the concept of the chemical capacitance reported in the MIEC electrode literature.[35,36] The chemical capacitance originates from a capacitive process related to the accumulation of electro-active oxygen species ($V_o^{\bullet\bullet}$) in the bulk of the electrode. It is therefore proportional to the thickness-area product of the electrode (volume) and the ease by which it changes stoichiometry. Because the chemical capacitance is related to the oxygen nonstoichiometry change of the oxide film, one can estimate a value for it from the STF thermodynamic data.[18,37] Considering that the effective chemical potential change induced by an ac amplitude of 20 mV corresponds to a ratio $pO_2/pO_{2,air} = 2.73$ change in oxygen partial pressure at 650°C via the Nernst equation, one can estimate a variation of ~0.3% in the total lattice oxygen.[21] Applying the expression of the chemical capacitance in terms of stoichiometry change δ with pO_2[37]

Table II. Surface exchange coefficient, bulk diffusion coefficient, electronic (σ_{el}) and ionic (σ_{ion}) conductivity, and electronic transfer number at 800°C for $SrTi_{1-x}Fe_xO_3$ (x = 0.13,[34] 35, and 50) and $La_{0.6}Sr_{0.4}Co_{0.2}Fe_{0.8}O_3$.[11,38]

	k (cm/s)	D (cm^2/s)	σ_{el} (S/cm)	σ_{ion} (S/cm)	t_e
STF35	2.0×10^{-5}	1.0×10^{-7}	9.9×10^{-1}	3.5×10^{-2}	0.9659
STF50	1.7×10^{-5}	1.1×10^{-7}	1.8	3.6×10^{-2}	0.9804
STF0.13	1.0×10^{-7}	2.0×10^{-9}	N/A	N/A	N/A
$La_{0.6}Sr_{0.4}Co_{0.2}Fe_{0.8}O_3$	5.6×10^{-6}	2.5×10^{-8}	302	8×10^{-3}	0.9997

$$C_\delta = -\frac{4F^2L}{V_m}\frac{d\delta}{d\mu_{O,\text{eff}}} = \frac{8F^2L}{RTV_m}\frac{d\delta}{d\ln P_{O_{2,\text{eff}}}} \quad [4]$$

in which F is the Faraday constant, L is the thickness of the film, and V_m is the molar volume of the oxide, one estimates a value of ~ 36 mF/cm^2 at 160 nm, in reasonable agreement with the measured value of ~ 12 mF/cm^2 in this work.

Conclusions

The STF model cathode, prepared as a dense film with well-defined area and thickness, was demonstrated to exhibit typical MIEC behavior with the electrode reaction occurring over the full electrode surface area rather than being limited to the TPB. The electrode impedance was observed to be independent of electrode thickness and inversely proportional to the square of the electrode diameter, pointing to surface exchange rather than bulk diffusion limited kinetics. Furthermore, a CGO interlayer was found to have a negligible effect on electrode impedance, eliminating oxygen transfer across the electrode/electrolyte interface as the rate limiting step.

The STF model cathode showed surprisingly low ASR between 570 and 650°C. Values for the surface exchange coefficient, k, were calculated and found to be comparable in magnitude to those exhibited by other popular mixed conductors such as LSC and LSCF, thereby confirming the suitability of STF as a model mixed conducting cathode material. This was in spite of the fact that the electronic conductivity of STF was several orders of magnitude lower than the other popular mixed conductors.

The large measured chemical capacitance ($\sim 10^{-2}$ F) was found to be consistent with an expected large electrochemically induced change in stoichiometry of the STF35 and STF50 electrodes. Studies are being extended to other values of x in STF to aid in obtaining an improved understanding of the correlation of electrochemical performance with material parameters such as electronic and an ionic conductivity and nonstoichiometry.

Acknowledgments

This work was supported by the National Science Foundation material world network collaboration under grant no. DMR-0243993 and originally initiated by the Department of Energy under grant no. DE-FC26-05NT42624. This work made use of the Shared Experimental Facilities supported by the MRSEC Program of the National Science Foundation under grant no. DMR 02-13282. The authors thank Professor E. Ivers-Tiffée's group, University of Karlsruhe, and Dr. A. Rothschild, Technion, for providing detailed STF defect chemical data and constructive discussion, and Professor Caroline A. Ross's group, MIT for use of the PLD system. The authors also thank the Samsung Scholarship for financial support.

Massachusetts Institute of Technology assisted in meeting the publication costs of this article.

References

1. N. Q. Minh, *J. Am. Ceram. Soc.*, **76**, 563 (1993).
2. J. Fleig, H. L. Tuller, and J. Maier, *Solid State Ionics*, **174**, 261 (2004).
3. M. Liu, *J. Electrochem. Soc.*, **145**, 142 (1998).
4. G. W. Coffey, L. R. Pederson, and P. C. Rieke, *J. Electrochem. Soc.*, **150**, A1139 (2003).
5. S. B. Adler, *JAMA, J. Am. Med. Assoc.*, **104**, 4791 (2004).
6. M. Prestat, J.-F. Koenig, and L. J. Gauckler, *J. Electroceram.*, **18**, 87 (2007).
7. S. B. Adler, J. A. Lane, and B. C. H. Steele, *J. Electrochem. Soc.*, **143**, 3554 (1996).
8. V. Dusastre and J. A. Kilner, *Solid State Ionics*, **126**, 163 (1999).
9. M. J. Jorgensen and M. Mogensen, *J. Electrochem. Soc.*, **148**, A433 (2001).
10. Z. Shao and S. M. Haile, *Nature (London)*, **431**, 170 (2004).
11. H. Ullmann, N. Trofimenko, F. Tietz, D. Stöver, and A. Ahmad-Khanlou, *Solid State Ionics*, **138**, 79 (2000).
12. A. Petric, P. Huang, and F. Tietz, *Solid State Ionics*, **135**, 719 (2000).
13. L.-W. Tai, M. M. Nasrallah, H. U. Anderson, D. M. Sparlin, and S. R. Sehlin, *Solid State Ionics*, **76**, 259 (1995).
14. L.-W. Tai, M. M. Nasrallah, H. U. Anderson, D. M. Sparlin, and S. R. Sehlin, *Solid State Ionics*, **76**, 273 (1995).
15. Y. L. Yang, C. L. Chen, S. Y. Chen, C. W. Chu, and A. J. Jacobson, *J. Electrochem. Soc.*, **147**, 4001 (2000).
16. A. Bieberle, L. P. Meier, and L. J. Gauckler, *J. Electrochem. Soc.*, **148**, A646 (2001).
17. J. L. Hertz and H. L. Tuller, *J. Electroceram.*, **13**, 663 (2004).
18. F. S. Baumann, J. Fleig, H.-U. Habermeier, and J. Maier, *Solid State Ionics*, **177**, 1071 (2006).
19. L. H. Brixner, *Mater. Res. Bull.*, **3**, 299 (1968).
20. G. M. Choi H. L. Tuller, and D. Goldschmidt, *Phys. Rev. B*, **34**, 6972 (1986).
21. A. Rothschild, W. Menesklou, H. L. Tuller, and E. Ivers-Tiffée, *Chem. Mater.*, **18**, 3651 (2006).
22. M. V. Patrakeev, I. A. Leonidov, V. L. Kozhevnikov, and V. V. Kharton, *Solid State Sci.*, **6**, 907 (2004).
23. A. Rothschild and H. L. Tuller, *J. Electroceram.*, **17**, 1005 (2006).
24. K. Sahner, R. Moos, M. Matam, J. J. Tunney, and M. Post, *Sens. Actuators B*, **108**, 102 (2005).
25. J. Fleig, *Solid State Ionics*, **150**, 181 (2002).
26. P. S. Manning, J. D. Sirman, R. A. De Souza, and J. A. Kilner, *Solid State Ionics*, **100**, 1 (1997).
27. H. Huang, M. Nakamura, P. C. Su, R. Fasching, Y. Saito, and F. B. Prinz, *J. Electrochem. Soc.*, **154**, B20 (2007).
28. H. Yokokawa, N. Sakai, T. Horita, K. Yamaji, and M. E. Brito, *MRS Bull.*, **30**, 591 (2005).
29. F. S. Baumann, J. Fleig, G. Cristiani, B. Stuhlhofer, H.-U. Habermeier, and J. Maier, *J. Electrochem. Soc.*, **154**, B931 (2007).
30. J. Jamnik, J. Maier, and S. Pejovnik, *Electrochim. Acta*, **44**, 4139 (1999).
31. J. Maier, *Physical Chemistry of Ionic Materials*, Wiley, Chichester (2004).
32. B. C. H. Steele, *Solid State Ionics*, **75**, 157 (1995).
33. R. A. De Souza, *Phys. Chem. Chem. Phys.*, **8**, 890 (2006).
34. M. Leonhardt, R. A. De Souza, J. Claus, and J. Maier, *J. Electrochem. Soc.*, **149**, J19 (2002).
35. J. Jamnik and J. Maier, *Phys. Chem. Chem. Phys.*, **3**, 1668 (2001).
36. J. Jamnik and J. Maier, *J. Electrochem. Soc.*, **146**, 4183 (1999).
37. T. Kawada, J. Suzuki, M. Sase, A. Kaimai, K. Yashiro, Y. Nigara, J. Mizusaki, K. Kawamura, and H. Yugami, *J. Electrochem. Soc.*, **149**, E252 (2002).
38. S. J. Benson, R. J. Chater, and J. A. Kilner, in *Proceedings of the 3rd International Symposium on Ionic and Mixed Conducting Ceramics*, PV 97–24, p. 596, The Electrochemical Society Proceedings Series, Pennington, NJ (1997).